bioRxiv preprint first posted online Jun. 20, 2018; doi: http://dx.doi.org/10.1101/352666. The copyright holder for this preprint (which was not peer-reviewed) is the author/funder. All rights reserved. No reuse allowed without permission.

Communication and quorum sensing in non-living mimics of eukaryotic cells

Henrike Niederholtmeyer[1], Cynthia Chaggan[1], and Neal K. Devaraj[1]*

[1]Department of Chemistry and Biochemistry, University of California, San Diego, USA.

*Correspondence to: ndevaraj@ucsd.edu

Abstract

Cells in tissues or biofilms communicate with one another through chemical and mechanical signals to coordinate collective behaviors. Non-living cell mimics provide simplified models of natural systems, however, it has remained challenging to implement communication capabilities comparable to living cells. Here we present a porous artificial cell-mimic containing a nucleus-like DNA-hydrogel compartment that is able to express and display proteins, and communicate with neighboring cell-mimics through diffusive protein signals. We show that communication between cell-mimics allowed distribution of tasks, quorum sensing, and cellular differentiation according to local environment. Cell-mimics could be manufactured in large quantities, easily stored, chemically modified, and spatially organized into diffusively connected tissue-like arrangements, offering a means for studying communication in large ensembles of artificial cells.

Main Text:

In communities of single-celled and multicellular organisms, cell-cell communication enables cells to organize in space, distribute tasks, and to coordinate collective responses. Communicating cells have been engineered to form cellular patterns (*1*, *2*) and synchronize gene expression (*3*). While biochemical reactions in microfluidic chambers and on beads can model aspects of intercellular communication (*4*, *5*), studies on non-living cell-mimics that structurally resemble natural cells have focused on single, isolated cell-mimics because of limitations in assembly methods and communication channels. To address the scalable assembly of artificial cells, microfluidic methods have been developed to mass-produce phospholipid vesicles encapsulating active biomolecules (*6-8*). Recent studies have demonstrated signaling between cell-mimics to induce gene expression (*9-11*) or chemical reactions (*12*, *13*) but signaling molecules have been limited to small molecules that can either freely cross membranes or require alpha-hemolysin pores. In contrast, signaling in multicellular organisms often involves secretion of proteins serving as growth factors or morphogens that provide cells with the information they need to develop into functional tissues (*14*).

bioRxiv preprint first posted online Jun. 20, 2018; doi: http://dx.doi.org/10.1101/352666. The copyright holder for this preprint (which was not peer-reviewed) is the author/funder. All rights reserved. No reuse allowed without permission.

Here, we prepared porous cell-mimics capable of gene expression and communication via diffusive protein signals using a microfluidic method (**Fig. 1, A and B,** Materials and Methods). First, water-in-oil-in-water double emulsion droplets were formed in a polydimethylsiloxane (PDMS) device (fig. S1, movie 1). The droplets had a middle organic phase consisting of a 1-decanol and acrylate monomer solution and encapsulated DNA and clay minerals. Second, double emulsion droplets were collected and polymerized using UV light, inducing a phase separation of the inert 1-decanol to form porous microcapsules (*15*). Third, following polymerization, we simultaneously permeabilized the polymer membrane and induced formation of a clay-hydrogel in their interior by adding a solution of ethanol and HEPES buffer. Membrane pores had diameters of 200-300 nm (**Fig. 1A**, fig. S2). Polymer membranes were permeable to macromolecules up to 2 MDa but excluded 220 nm nanoparticles from about 90% of the microcapsules (fig. S3). The clay hydrogel trapped DNA in the interior of the porous microcapsules (fig. S4) (*16*) in a structure that is analogous to the cell nucleus (**Fig. 1C**, fig. S5). The clay-DNA hydrogel partially excluded 2 MDa dextran but smaller macromolecules could enter (fig. S3). Fourth, to prevent non-specific binding of proteins to the polymer membrane of cell-mimics we passivated their surface with polyethylene glycol (PEG) (fig. S6).

The porous structure of the polymer membrane allowed supply of cell-free transcription and translation (TX-TL) reagents from the outside to induce synthesis of proteins encoded by the DNA in the cell-mimics' hydrogel nuclei. Even ribosomes, the largest components of TX-TL reagents, were able to diffuse into cell-mimics through their porous membranes (fig. S7). To capture protein products within cell-mimics we expressed a fusion protein of the tetracycline repressor TetR and sfGFP (TetR-sfGFP) as a fluorescent reporter. TetR binds the *tet* operator sequence (*tetO*). A co-encapsulated 240x *tetO* array plasmid localized the reporter protein to the hydrogel nucleus (**Fig. 1C**), which increased in fluorescence after TX-TL addition (**Fig. 1D**, movie 2). Localization of TetR-sfGFP to the hydrogel nucleus was reversible and due to the specific interaction of TetR with *tetO* sites. Addition of anhydrotetracyline, which prevents TetR from binding DNA, caused a substantial unbinding of TetR-sfGFP. Without the *tetO* plasmid, fluorescence increased in solution but not in hydrogel nuclei (fig. S8). In *tetR*-sfGFP / *tetO* cell-mimics, fluorescence increased substantially in almost all cell-mimics (**Fig. 1E**). Variations in intensity were likely due to differences in DNA capture during formation of hydrogel nuclei (fig. S5). Compared to lipid vesicles, polymeric cell-mimics are easier to work with and more stable. Unlike lipid vesicles, the cell-mimics reported here were easily transferred into new media, retained full expression capabilities after two years of storage, and separate batches showed comparable expression levels and dynamics (fig. S9).

Due to their porosity, cell-mimics likely released mRNA and protein products that diffused into neighboring cell-mimics. To demonstrate that neighboring cell-mimics exchanged protein products with each other, we prepared "sender" cell-mimics, fluorescently labeled in their polymeric membranes and containing the *tetR*-sfGFP expression plasmid, and "receiver" cell-mimics containing the *tetO* array plasmid to capture the reporter protein. When both cell-mimic types were mixed at approximately a

bioRxiv preprint first posted online Jun. 20, 2018; doi: http://dx.doi.org/10.1101/352666. The copyright holder for this preprint (which was not peer-reviewed) is the author/funder. All rights reserved. No reuse allowed without permission.

one to one ratio, only the nuclei of the receiver cell-mimics increased in fluorescence (**Fig. 2A**). To explore how far TetR-sfGFP protein originating from a given sender cell-mimic travelled, we used a large excess of receivers and spread them densely into a circular 3.5 mm wide "colony". Under these conditions, TetR-sfGFP spread from sender to surrounding receiver cell-mimics but stayed localized in patches around individual sender cell-mimics (**Fig 2B**, fig. S10A). This pattern of captured protein around source cell-mimics persisted for 24 h after expression ended, demonstrating that TetR-sfGFP was essentially trapped in the hydrogel nuclei once it was bound in the high local density of *tetO* sites. Assuming free diffusion, we would expect protein gradients to have disappeared within 5 h in similar geometries (fig. S10B-D).

To test the preference of a given cell-mimic to bind protein originating from its own DNA, we prepared *tetR*-mCherry / *tetO* cell-mimics that accumulated red fluorescence in their hydrogel nuclei (fig. S10). When mixed with *tetR*-sfGFP / *tetO* cell-mimics (**Fig. 1C**), there was essentially no difference in relative fluorescence in either channel between the cell-mimic types, indicating that in close proximity, neighboring cell-mimics completely exchanged protein products (fig. S11). While transcription occurred in the hydrogel nuclei where DNA was localized, these results indicate that translation was likely not localized to the cell-mimic a given mRNA originated from. However, because mRNA lifetime in TX-TL reagents is short, and mRNA thus has a limited diffusion range, we expected the localization of TetR-sfGFP and TetR-mCherry to depend strongly on distance between cell-mimics. We distributed the two cell-mimic types in a reaction chamber so that they mixed in the center but remained separate on either side. Cell-mimics in the center showed mixed fluorescence while cell-mimics on the sides fluoresced primarily in one channel (**Fig. 2C**), demonstrating that locally, on the order of few cell-mimic lengths, proteins exchanged with little hindrance by the polymer membranes, whereas exchange of protein with distant cell-mimics was limited by diffusion.

Communication in vesicle-based cell-mimics has so far been limited to small molecule signals such as IPTG and glucose, combined with membrane pores, like alpha-hemolysin (*9*, *13*). Our porous cell-mimics exchanged proteins with their neighbors, suggesting they are able to communicate with each other directly through genetic regulators. To demonstrate this we constructed a two-stage activation cascade and distributed the network into two separate cell-mimic types. T3 RNA polymerase (T3 RNAP) served as a diffusive signaling molecule transmitting the instruction to express a reporter gene from "activator" to "reporter" cell-mimics. Activator cell-mimics contained the template for the expression of T3 RNAP. Reporter cell-mimics contained the template for the T3 RNAP-driven synthesis of the TetR-sfGFP reporter as well as *tetO* array plasmids to capture the reporter protein. When both cell-mimic types were mixed, reporter cell-mimics expressed and bound the fluorescent reporter (**Fig. 3**, movie 3), while activator cell-mimics alone did not increase in fluorescence (fig. S12).

We hypothesized that T3 RNAP could serve as a soluble signaling molecule providing cell-mimics with information about population density. Indeed, cell-mimics containing both the activation circuit and reporter constructs (**Fig. 4A**) underwent a collective

bioRxiv preprint first posted online Jun. 20, 2018; doi: http://dx.doi.org/10.1101/352666. The copyright holder for this preprint (which was not peer-reviewed) is the author/funder. All rights reserved. No reuse allowed without permission.

response where fluorescence accumulated in cell-mimics only at high densities. At low cell-mimic densities, signals from the hydrogel nuclei were not detectably different from background fluorescence (**Fig. 4B**). We titrated the density of cell-mimics in a fixed volume and found a sharp transition from "off" to "on," which resembled bacterial quorum sensing responses to cell density (*17*). The threshold cell-mimic density at which expression of the reporter turned on was 400 cell-mimics in 4.5 μl TX-TL (**Fig. 4C**). Cell-mimics that constitutively expressed the reporter (**Fig. 1C**) accumulated fluorescence in their hydrogel nuclei regardless of their density (fig. S13). The collective response to density can be explained by T3 RNAP release from cell-mimics. At low densities, T3 RNAP is diluted in the comparably large volume of the sample, while at high density a sufficient concentration of transcriptional activator accumulates to turn on expression of the reporter. Titrating the T3 RNAP template DNA in TX-TL reactions, we found a similarly sharp transition in expression with a half-maximal activation at 10 pM (fig. S14). The calculated bulk concentration of T3 RNAP template in an artificial quorum sensing experiment at the threshold density of 400 cell-mimics per droplet is 12.5 pM. In contrast to bacterial quorum sensing (*17*), the mechanism of our artificial quorum sensing involved no positive feedback loop and employed a protein instead of a small molecule, showing that artificial cells can model biological phenomena using unnatural parts and mechanisms.

During development, cells interpret signals secreted by their neighbors to differentiate into specialized cell-types that express different sets of genes (*14*). We aimed to mimic cellular differentiation according to local environment by combining the artificial quorum sensing network with a constitutively expressed *tetR*-mCherry reporter that turns on irrespective of cell-mimic density (**Fig. 4D**). We distributed cell-mimics unevenly in a long narrow reaction chamber (**Fig. 4E**), and analyzed the fluorescence of individual hydrogel nuclei according to their location in the density gradient. While absolute fluorescence intensities and background fluorescence increased with cell-mimic density, hydrogel nuclei from the high density area displayed visibly higher sfGFP:mCherry ratios than hydrogel nuclei in the dilute region that primarily displayed mCherry fluorescence (**Fig. 4F**). In the continuous density gradient we observed some graded responses in the center of the chamber at medium density. However, plotting sfGFP against mCherry fluorescence for individual hydrogel nuclei revealed two distinct populations of fluorescence signals according to position in the chamber (fig. S15).

Our system has a number of potential uses, including programming cell-mimics to collectively sense and respond to their local environment. As translation of proteins takes place inside and outside of the cell-mimic, and mRNAs and proteins can freely diffuse, our system might model features of the syncytium stage of *Drosophila* embryogenesis (*18*), including the nuclear trapping responsible for establishing sharp gradients of phosphorylated ERK/MAPK (dpERK) across the syncytical *Drosophila* embryo by limiting diffusion of dpERK (*19*). Genetic circuits could be distributed into separate cell-mimics, which allowed them to share tasks. Such modularity might facilitate prototyping of gene circuits by titrating cell-mimics containing different parts of a network. Furthermore, individual components of circuits located in different cell-mimics can be spatially organized to generate spatiotemporal expression patterns. Indeed, artificial cell-

bioRxiv preprint first posted online Jun. 20, 2018; doi: http://dx.doi.org/10.1101/352666. The copyright holder for this preprint (which was not peer-reviewed) is the author/funder. All rights reserved. No reuse allowed without permission.

mimics could be used to develop sensors and self-organizing materials, as well as being arrayed into synthetic tissues of artificial cells, which could serve as simplified models for reaction-diffusion processes.

Materials and Methods:

Fabrication of microfluidic chips

A silicon wafer patterned with SU-8 photoresist served as a mold for PDMS devices. The mold was prepared following standard photolithography procedures to produce a feature height of 43 µm. Design of the flow focusing junction was adapted from Desphande et al. 2016 (*7*) (Fig. S1). PDMS (Sylgard, Dow Corning) was prepared at a 1:10 ratio and cured for 1h at 80°C. PDMS devices were bonded to PDMS spincoated cover glass using oxygen plasma (50 watt for 30 sec at 0.45 torr). After bonding, devices were baked overnight at 120°C to recover hydrophobicity. Channels downstream of the flow-focusing junction were rendered hydrophilic by a treatment with a 5% (wt/vol) polyvinyl alcohol (PVA) solution as described (*7*). Following PVA-treatment, devices were baked again for 2 h at 120°C and used immediately or stored for up to two months.

Production of porous cell-mimics with clay-DNA hydrogel nuclei

2 % (wt/vol) Laponite XLG (BYK Additives) clay stock was prepared by mixing 10 ml of ultrapure H_2O on a magnetic stir plate to create a vortex. 200 mg of Laponite XLG were slowly added into the vortex and left to stir for 2 h until clear. The dispersion was then stored at 4°C and used for up to a week. Photoinitiator 2,2-Dimethoxy-2-phenylacetophenone was dissolved at 5 % (wt/vol) in 1-decanol and in Trimethylolpropane ethoxylate triacrylate (ETPTA, Sigma-Aldrich, Mn 428). ETPTA with photoinitiator was stored at 4°C and used for up to a week. Double emulsion droplets were prepared with an inner aqueous solution (IA) containing 0.4 % (wt/vol) laponite XLG, 15 % (vol/vol) glycerol, 50 mg/ml poloxamer 188, 20 µM sulfo-Cy5 and up to 300 ng/µl plasmid or linear DNA. The middle organic phase (MO) was composed of glycidyl methacrylate (GMA, Sigma-Aldrich), ETPTA, and 1-decanol at a 48:32:20 ratio and contained 2.6 % (wt/vol) photoinitiator and 0.25 % (vol/vol) Span-80 to produce porous microcapsules (*15*). For fluorescently labeled microcapsule membranes, the MO phase contained 0.1 mg/ml Methacryloxyethyl thiocarbamoyl rhodamine B. The outer aqueous phase (OA) was 15 % (vol/vol) glycerol with 50 mg/ml poloxamer 188. Using syringe pumps, the three phases were flowed through the microfluidic device at speeds of 3 to 12 µl/hr for the IA, 30 to 70 µl/hr for the MO and 250 to 500 µl/hr for the OA phase. Flow rates were adjusted to produce a stable formation of double emulsion droplets and then left unchanged for collection of droplets. Typically, about 200 µl of double emulsion were collected from the chip. The emulsion was then placed in a 2mm thick chamber built from cover glass and exposed to 350 nm UV light for 30 seconds using a UV reactor (Rayonet). The dispersion of polymerized microcapsules was then added to 2 ml solution of 70 % Ethanol containing 200 mM HEPES pH 8 to permeabilize the shell and to form the DNA-clay hydrogel nucleus. This stock was stored at -20°C until use.

bioRxiv preprint first posted online Jun. 20, 2018; doi: http://dx.doi.org/10.1101/352666. The copyright holder for this preprint (which was not peer-reviewed) is the author/funder. All rights reserved. No reuse allowed without permission.

To prevent non-specific binding of proteins to porous polymer membranes, microcapsules were treated with polyethylene glycol (PEG). We coupled amino-PEG12-alcohol to the epoxide functionalities on the polymer shells. First, microcapsules were washed with 200 mM sodium carbonate buffer pH 10 by centrifugation. All supernatant was removed from the capsule pellet and a solution of 250mM amino-PEG12-alcohol in 50% ethanol pH 10 was added to the pellet. Microcapsules were incubated at 37°C for reaction overnight and then washed with 100 mM HEPES pH 8. These PEGylated cell-mimics were either used directly or stored in 70 % ethanol 200 mM HEPES pH 8 at -20°C.

DNA templates

Plasmids used in this study are listed in Table S1. Plasmid DNA was purified using the NucleoBond Xtra Midi kit (Macherey-Nagel), followed by an isopropanol precipitation and resuspension of the DNA pellet in ultrapure H_2O to prepare highly concentrated plasmid stocks and maximize expression in TX-TL reactions. The template for T3 RNA polymerase was on linear DNA prepared by PCR from a plasmid template. DNA template concentrations encapsulated in cell-mimics are listed in Table S2.

Cell-free transcription and translation reactions

E. coli lysate for TX-TL reactions was prepared by freeze-thawing from *E. coli* BL21-Gold (DE3)/pAD-LyseR (*20*). To induce T7 RNA polymerase activity besides *E. coli* RNA polymerase activity the main culture was induced with 0.5mM IPTG an optical density measured at 600 nm (OD_{600}) of 0.5-0.6. Cells were harvested by centrifugation at an OD_{600} of 1.4. Processing of the lysate was performed as described (*20*). For the final composition of TX-TL reactions, cell lysate was diluted 2.5-fold with reaction buffer, microcapsules or DNA, and other additions as needed. This resulted in the following concentrations in the TX-TL reaction: 4.6 mg/ml protein, 7 mM Mg-glutamate, 60 mM K-glutamate, 3.5 mM DTT, 0.75 mM each amino acid except leucine, 0.63 mM leucine, 50 mM HEPES, 1.5 mM ATP and GTP, 0.9 mM CTP and UTP, 0.2 mg/mL tRNA, 0.26 mM CoA, 0.33 mM NAD, 0.75 mM cAMP, 0.068 mM folinic acid, 1 mM spermidine, 30 mM 3-PGA, 3.5% PEG-8000. When linear DNA templates were used, they were stabilized by adding 4 µM of chi6 duplex DNA to the TX-TL reaction (*21*). TX-TL reactions were incubated at 29°C for expression.

Gene expression in cell-mimics

For cell-mimics, expression reactions typically consisted of 1 µl concentrated cell-mimics in 100 mM HEPES pH 8 and TX-TL reagents for a final volume of 5 µl. Droplets of 4.5 µl of this mixture were pipetted onto a 35 mm Lumox dish (Sarstedt). The gas permeable substrate ensured homogeneous sfGFP expression in the sample. The cell-mimic droplet was covered with cover glass and sealed with a ring of vacuum grease to prevent evaporation and provide a spacer. The reaction volume was scaled up for experiments in larger samples, and was 20 µl in Fig. 2b and 35 µl for long, narrow reaction chambers in Fig. 2c and Fig. 4e. Long, narrow reaction chambers were made from two parallel 20 mm lines of vacuum grease with a gap of 2 mm, which was filled with TX-TL and cell-mimics and then sealed with cover glass.

bioRxiv preprint first posted online Jun. 20, 2018; doi: http://dx.doi.org/10.1101/352666. The copyright holder for this preprint (which was not peer-reviewed) is the author/funder. All rights reserved. No reuse allowed without permission.

Preparation of labeled ribosomes

E. coli ribosomes (New England Biolabs) were incubated in labeling buffer (50 mM HEPES pH 8.2, 100 mM KCl, 10 mM magnesium acetate) with a molar excess of Alexa Fluor 488 NHS Ester (ThermoFisher Scientific) for 90 min at room temperature. Free dye was removed by washing with labeling buffer in centrifugal filter devices with a molecular weight cut-off of 100 kDa. Each ribosome contained approximately eleven Alexa Fluor 488 labels.

Plate reader reactions

Plate reader reactions were performed in 384-well plates using a 10 µl reaction volume covered with 10 µl light mineral oil in a Tecan infinite F200 plate reader. GFP fluorescence was read every 5 min using a 485 nm ± 20 nm excitation filter and a 550 nm ± 35 nm emission filter, followed by 1 min of shaking. Fluorescence intensity measurements were calibrated using purified sfGFP-His_6 to determine absolute concentrations.

Imaging and image analysis

Images were acquired using a spinning disk confocal microscope consisting of a Yokagawa spinning disk system (Yokagawa, Japan) built around an Axio Observer Z1 motorized inverted microscope (Carl Zeiss Microscopy GmbH, Germany) with a 20x 1.42 NA objective. Large regions were imaged as tiles and stitched using ZEN Blue software. Further image processing and analyses were done in Fiji/ImageJ (*22*). Fluorescence traces or endpoint intensities of individual hydrogel nuclei were extracted from timelapse movies by measuring fluorescence in manually selected oval regions in nuclei, using a non-fluorescent region in each cell-mimic for background subtraction. Artificial quorum sensing data was analyzed using the colony counter plugin in Fiji/ImageJ to segment and count cell-mimics and polymer beads in the stitched brightfield image of a droplet. When necessary, regions of interest were manually added or deleted. Fluorescence values of individual cell-mimics were mean fluorescence values of the individual segmented cell-mimics. For background correction, fluorescence values of segmented regions from each droplet were sorted. The lowest fluorescence intensities were from solid polymer beads, and we used this property for background correction. We removed the lowest 34 % of values, which was the percentage of polymer beads in the sample, and used the highest of the removed values for background subtraction of the reduced list.

Experiments (each analyzed droplet with different amounts of cell-mimics) were performed for densities between 25 and 800 cell-mimics per droplet, which were binned every 50 cell-mimics. Each bin contained data from at least 156 analyzed cell-mimics. Scanning electron microscopy was performed with a Zeiss SIGMA VP field emission scanning electron microscope using air-dried cell-mimics. To image cross sections of microcapsule polymer membranes, cell-mimics were cut using a razor blade.

References:

1. S. Basu, Y. Gerchman, C. H. Collins, F. H. Arnold, R. Weiss, A synthetic multicellular system for programmed pattern formation. *Nature*. **434**, 1130–1134 (2005).

bioRxiv preprint first posted online Jun. 20, 2018; doi: http://dx.doi.org/10.1101/352666. The copyright holder for this preprint (which was not peer-reviewed) is the author/funder. All rights reserved. No reuse allowed without permission.

2. L. Morsut *et al*., Engineering Customized Cell Sensing and Response Behaviors Using Synthetic Notch Receptors. *Cell*. **164**, 780–791 (2016).

3. T. Danino, O. Mondragón-Palomino, L. Tsimring, J. Hasty, A synchronized quorum of genetic clocks. *Nature*. **463**, 326–330 (2010).

4. A. M. Tayar, E. Karzbrun, V. Noireaux, R. H. Bar-Ziv, Propagating gene expression fronts in a one-dimensional coupled system of artificial cells. *Nat Phys*, 1037–1041 (2015).

5. G. Gines *et al*., Microscopic agents programmed by DNA circuits. *Nature Nanotechnology*. **12**, 351–359 (2017).

6. D. van Swaay, A. deMello, Microfluidic methods for forming liposomes. *Lab Chip*. **13**, 752 (2013).

7. S. Deshpande, Y. Caspi, A. E. C. Meijering, C. Dekker, Octanol-assisted liposome assembly on chip. *Nature Communications*. **7**, 10447 (2016).

8. N.-N. Deng, M. Yelleswarapu, L. Zheng, W. T. S. Huck, Microfluidic Assembly of Monodisperse Vesosomes as Artificial Cell Models. *J Am Chem Soc*. **139**, 587–590 (2017).

9. K. P. Adamala, D. A. Martin-Alarcon, K. R. Guthrie-Honea, E. S. Boyden, Engineering genetic circuit interactions within and between synthetic minimal cells. *Nature Chemistry*. **9**, 431–439 (2017).

10. R. Lentini *et al*., Two-Way Chemical Communication between Artificial and Natural Cells. *ACS Cent. Sci*. **3**, 117–123 (2017).

11. G. Rampioni *et al*., Synthetic cells produce a quorum sensing chemical signal perceived by Pseudomonas aeruginosa. *Chem. Commun. (Camb.)*. **54**, 2090–2093 (2018).

12. S. Sun *et al*., Chemical Signaling and Functional Activation in Colloidosome-Based Protocells. *Small*. **12**, 1920–1927 (2016).

13. T. Y. D. Tang *et al*., Gene-Mediated Chemical Communication in Synthetic Protocell Communities. *ACS Synth. Biol*. **7**, 339–346 (2018).

14. M. A. Basson, Signaling in Cell Differentiation and Morphogenesis. *Cold Spring Harbor Perspectives in Biology*. **4**, a008151–a008151 (2012).

15. B. Kim, T. Y. Jeon, Y.-K. Oh, S.-H. Kim, Microfluidic Production of Semipermeable Microcapsules by Polymerization-Induced Phase Separation. *Langmuir*. **31**, 6027–6034 (2015).

16. D. Yang *et al*., Enhanced transcription and translation in clay hydrogel and

bioRxiv preprint first posted online Jun. 20, 2018; doi: http://dx.doi.org/10.1101/352666. The copyright holder for this preprint (which was not peer-reviewed) is the author/funder. All rights reserved. No reuse allowed without permission.

implications for early life evolution. *Sci Rep*. **3**, 3165 (2013).

17. W.-L. Ng, B. L. Bassler, Bacterial Quorum-Sensing Network Architectures. *Annu. Rev. Genet*. **43**, 197–222 (2009).

18. D. S. Johnston, C. Nüsslein-Volhard, The origin of pattern and polarity in the Drosophila embryo. *Cell*. **68**, 201–219 (1992).

19. M. Coppey, A. N. Boettiger, A. M. Berezhkovskii, S. Y. Shvartsman, Nuclear Trapping Shapes the Terminal Gradient in the Drosophila Embryo. *Current Biology*. **18**, 915–919 (2008).

20. A. Didovyk, T. Tonooka, L. Tsimring, J. Hasty, Rapid and Scalable Preparation of Bacterial Lysates for Cell-Free Gene Expression. *ACS Synth. Biol*. **6**, 2198–2208 (2017).

21. R. Marshall, C. S. Maxwell, S. P. Collins, C. L. Beisel, V. Noireaux, Short DNA containing χ sites enhances DNA stability and gene expression in E. colicell-free transcription-translation systems. *Biotechnology and bioengineering*. **114**, 2137–2141 (2017).

22. J. Schindelin *et al*., Fiji: an open-source platform for biological-image analysis. *Nat Meth*. **9**, 676–682 (2012).

23. M. T. Tyn, T. W. Gusek, Prediction of diffusion coefficients of proteins. *Biotechnology and bioengineering*. **35**, 327–338 (1990).

24. S. P. Finney-Manchester, N. Maheshri, Harnessing mutagenic homologous recombination for targeted mutagenesis in vivo by TaGTEAM. *Nucleic Acids Res*. **41**, e99–e99 (2013).

Acknowledgements:

This work was supported by the Department of Defense (Army Research Office) through the Multidisciplinary University Research Initiative (MURI), award W911NF-13-1-0383. H. N. was supported by a Swiss National Science Foundation fellowship. We thank Lev Tsimring, Partho Ghosh and Andrew Rudd for helpful comments on the manuscript, Ahanjit Bhattacharya for labeled ribosomes, Andriy Didovyk for *E. coli* strain BL21-Gold (DE3)/pAD-LyseR, and Prof. Jeff Hasty and Ryan Johnson for their collaboration in microfluidic chip fabrication. We thank the UCSD School of Medicine Microscopy Core with grant NS047101 and Jennifer Santini for assistance with scanning electron microscopy, and the Waitt Advanced Biophotonics Core Facility of the Salk Institute with funding from NIH-NCI CCSG: P30 014195, NINDS Neuroscience Core Grant: NS072031 and the Waitt Foundation. Authors declare no competing interests. All data is available in the main text or the supplementary materials.

bioRxiv preprint first posted online Jun. 20, 2018; doi: http://dx.doi.org/10.1101/352666. The copyright holder for this preprint (which was not peer-reviewed) is the author/funder. All rights reserved. No reuse allowed without permission.

Supplementary Materials

Materials and Methods
Figures S1 – S15
Tables S1 – S2
Movies S1 – S3

bioRxiv preprint first posted online Jun. 20, 2018; doi: http://dx.doi.org/10.1101/352666. The copyright holder for this preprint (which was not peer-reviewed) is the author/funder. All rights reserved. No reuse allowed without permission.

Figures and Figure legends

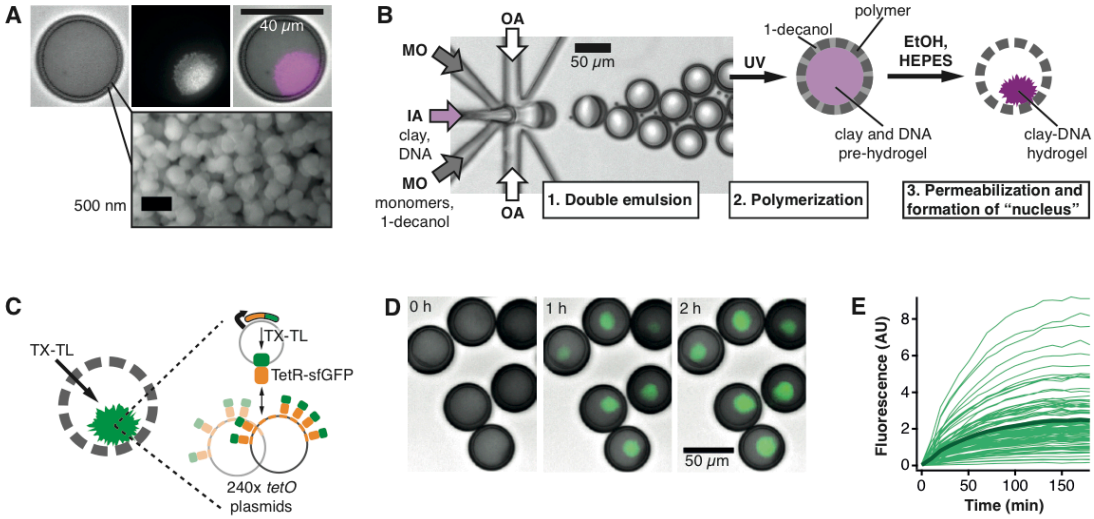

Fig. 1. Formation of cell-mimics containing artificial "nuclei" capable of gene expression.
A) Optical micrographs (top) of a cell-mimic with GelRed stained hydrogel "nucleus" (brightfield, red fluorescence, merge) and scanning electron microscopy of porous cell-mimic membrane (bottom). B) Microfluidic production of double emulsion droplets encapsulating a pre-hydrogel in a photocurable middle layer, and schematic of subsequent processing steps (see Materials and Methods). IA: Inner aqueous, MO: middle organic, OA: Outer aqueous phase. C) Schematic and timelapse images (D) of expression and capture of TetR-sfGFP in hydrogel nuclei (green, merged with brightfield images). TX-TL reagents were added at 0 h. E) Dynamics of fluorescence signal increase in the hydrogel nuclei of 100 cell-mimics with average shown in bold.

bioRxiv preprint first posted online Jun. 20, 2018; doi: http://dx.doi.org/10.1101/352666. The copyright holder for this preprint (which was not peer-reviewed) is the author/funder. All rights reserved. No reuse allowed without permission.

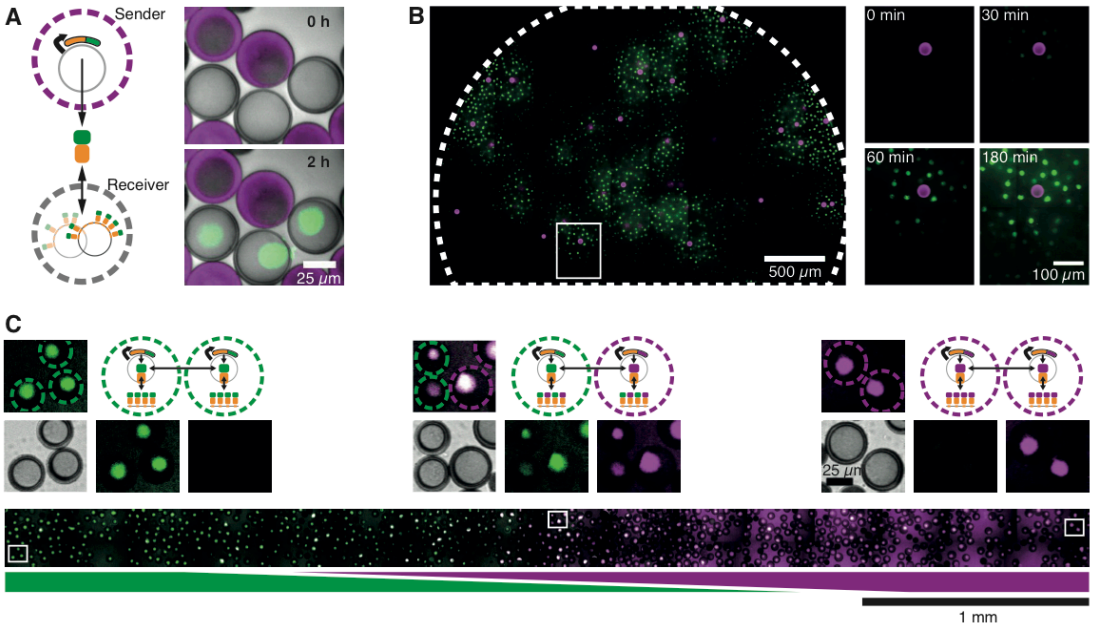

Fig. 2. Protein exchange between neighboring and distant cell-mimics.
A) Schematic of diffusive TetR-sfGFP exchange between neighboring sender and receiver cell-mimics and timelapse images of neighboring senders (rhodamine B stained membranes) and receivers (unstained membranes). Merge of brightfield and fluorescence channels (sender membranes, magenta; TetR-sfGFP, green). B) Distribution of TetR-sfGFP (green) in a dense droplet of receivers and sparse senders (magenta) after 3 h of expression. A small region around a sender (white box) is magnified and spreading of fluorescence is shown at different time points. C) Inhomogeneous mix of two types of cell-mimics producing and binding different color reporter proteins. *tetR*-sfGFP / *tetO* (green) and *tetR*-mCherry / *tetO* cell-mimics (magenta) were distributed in a channel to stay separate at the sides and mix in the center. Bottom image shows the distribution of sfGFP and mCherry fluorescence after 5 h. Merge of the two channels results in a white signal (middle). Magnified images from indicated positions along the channel are shown above. Merged image with cell-mimic types indicated by colored, dashed circles (top), and brightfield, sfGFP and mCherry signals shown separately (below).

bioRxiv preprint first posted online Jun. 20, 2018; doi: http://dx.doi.org/10.1101/352666. The copyright holder for this preprint (which was not peer-reviewed) is the author/funder. All rights reserved. No reuse allowed without permission.

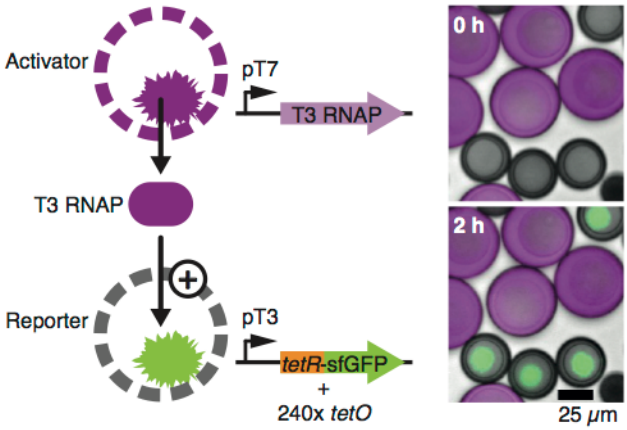

Fig. 3. Communication between cell-mimics via a diffusive genetic activator. Schematic of the two types of cell-mimics communicating through a distributed genetic activation cascade. Micrographs show a merge of brightfield images with rhodamine B fluorescence in the membranes of activators (magenta) and fluorescence of TetR-sfGFP (green) in the hydrogel nuclei of reporters directly after addition of TX-TL and after 2 h of expression.

bioRxiv preprint first posted online Jun. 20, 2018; doi: http://dx.doi.org/10.1101/352666. The copyright holder for this preprint (which was not peer-reviewed) is the author/funder. All rights reserved. No reuse allowed without permission.

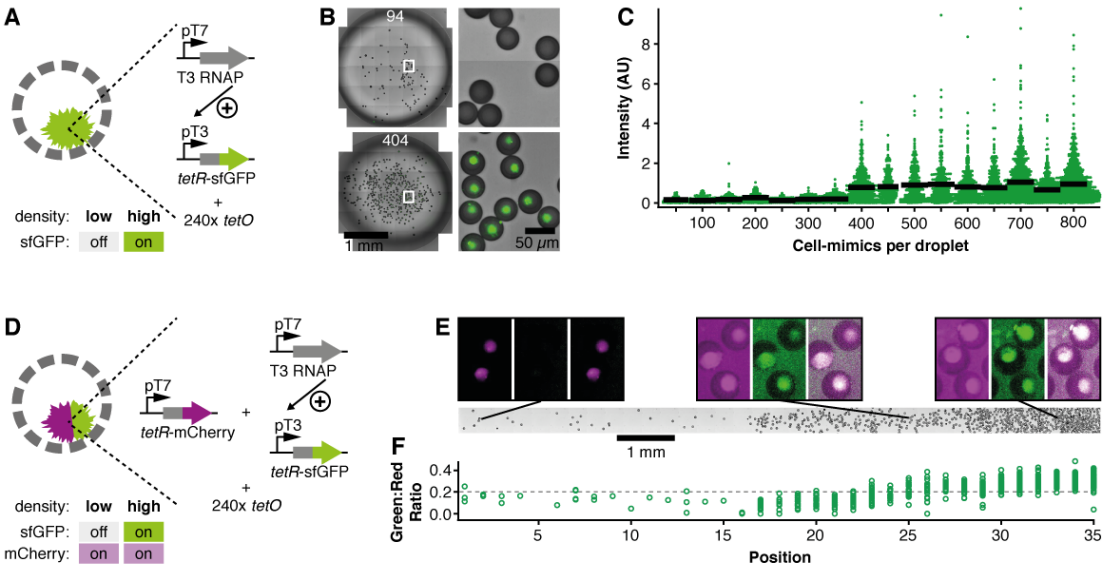

Fig. 4. Density sensing in populations of cell-mimics.
A) Artificial quorum sensing cell-mimics contain T3 activation cascade DNA templates and 240x *tetO* plasmids. B) Micrographs of cell-mimics in 4.5 μl droplets of TX-TL (left). The number of cell-mimics is indicated. Enlarged regions (indicated by white boxes) show presence and absence of fluorescence (green) in hydrogel nuclei after 3h of expression. C) Scatter dot plot of fluorescence intensities in individual cell-mimics at different densities. Each density category combines data in increments of 50 cell-mimics per droplet and contains data from at least 156 cell-mimics. Black bars show average fluorescence. D) A 2-color response to density is achieved by adding a constitutively expressed reporter (pT7-*tetR*-mCherry), which is "on" independent of density. E) 2-color density sensors were spread at increasing density in an elongated chamber (brightfield image, bottom). Panels above show magnified fluorescence images of indicated regions (mCherry fluorescence: magenta, left; sfGFP fluorescence: green, middle; merge of fluorescence channels: right). Images in each channel are window leveled to the same values and have a width of 70 μm. F) Ratio between sfGFP to mCherry fluorescence in individual hydrogel nuclei along the chamber. Positions correspond to tile regions of the image above.